Na^+ diffusion in $Na_xCo[Fe(CN)_6]_{0.90}$ film as investigated by transmission image

Hiroki Iwaizumi[1]. Takayuki Shibata[2], and Yutaka Moritomo[1,3,4]*

[1] *Graduate School of Pure & Applied Science, University of Tsukuba, Tennodai 1-1-1, Tsukuba, Ibaraki 305-8571, Japan*
[2] *Faculty of Marine Technology, Tokyo University of Marine Science and Technology, Etchujima 2-1-6, Koto-ku, Tokyo 135-8533, Japan*
[3] *Faculty of Pure & Applied Science, University of Tsukuba, Tennodai 1-1-1, Tsukuba, Ibaraki 305-8571, Japan*
[4] *Tsukuba Research Center for Energy Materials Science (TREMS), University of Tsukuba, Tennodai 1-1-1, Tsukuba, Ibaraki 305-8571, Japan*

Diffusion of alkali metal ions plays an important role on the rate property of battery. Here, we investigated macroscopic Na^+ diffusion in thin film of $Na_xCo[Fe(CN)_6]_{0.90}$ (NCF90) by means of transmitted light intensity image at 540 nm. The distribution of the Na^+ concentration (x) was determined against the elapsed time (t). We found that the diffusion constant (D) for Na^+ shows x-dependence as D = 6.0×10^{-8} - (1.6 - x)6.0×10^{-8} cm^2/s. The average D value (= 3.0×10^{-8} cm^2/s) is much larger than the reported value (= 0.5×10^{-10} cm^2/s[1)]) of $Na_xCo[Fe(CN)_6]_{0.88}$ (x = 0.8) determined by the electrochemical impedance spectroscopy. The large D value evaluated in the present investigation is ascribed to the fast intergrain diffusion process.

In lithium-ion (LIB) and sodium-ion (SIB) secondary batteries, diffusion of alkali metal ions in the electrode materials plays an important role on the rate property. To fabricate a battery with excellent rate property, development of electrode materials with large diffusion constant (D) is indispensable. The D value is usually evaluated by the electrochemical impedance spectroscopy (EIS) and analysis with the Randel's equivalent circuit model,[2)] which consists of electrolyte resistance, ionic charge-transfer resistance, double-layer capacitance, and restricted diffusion impedance. So far, the D values of many battery materials have been reported for Li^+ and Na^+. The D values for Li^+ is 10^{-12} - $10^{-11}cm^2/s$ in $LiCoO_2$[3)] with a layered rock-salt structure, 10^{-13} - $10^{-12}cm^2/s$ in $LiFePO_4$[4)] with an olivine structure, and 10^{-12} - $10^{-10}cm^2/s$ in $LiMn_2O_4$[5)] with a spinel structure. Shibata *et al.*[6)] reported the D value (= 4 - 9 × 10^{-11} cm^2/s) for Na^+ in P2-$NaCoO_2$ is comparable to the value (= 10^{-12} - $10^{-11}cm^2/s$) for Li^+ in $LiCoO_2$[3)] On the other hands, scanning probe microscopies (SPMs) are also poert ful tool to perform *ex situ* and *in situ* local characterization of battery materials.[7–14)] So far, local dynamics of Li^+ are reported by means of conductive atomic force microscopy (c-AFM),[7,8)] electrochemical strain microscopy (ESM),[8–10)] scanning electrochemical microscopy (SECM),[11,12)] and so on. By means of ESM approach, Yang *et al.*[9)] reported local D value (= 3×10^{-12} cm^2/s) for Li^+ in $Li_{1.2}Co_{0.13}Ni_{0.13}Mn_{0.54}O_2$ thin film. By means of SECM approach, Takahashi *et al.*[11)] reported local D value ($\sim 10^{-11}$ cm^2/s) for Li^+ in single $LiFePO_3$ particle.

Prussian blue analogues[15)] (PBA, $Li_xM[Fe(CN)_6]_y$ and $Na_xM[Fe(CN)_6]_y$; where M = Mn, Fe, Co, Ni, Fe, Cu, and Cd) are promising electrode materials for LIB[16–20)] and SIB.[21–31)] The compound consists of three-dimensional cyano-bridged jungle-gym-type framework and guest ions (Li^+ or Na^+). The guest ions are reversibly accommodated in the framework, causing material functionalities such as battery, gas storage, electrochromism, and so on. Importantly, PBAs exhibit large D values for Li^+ and Na^+,[1)] reflecting the robust and wide cyano-bridged framework. The D values for Li^+ were reported to be 4.6×10^{-10} cm^2/s in $Li_xMn[Fe(CN)_6]_{0.84}$ at x = 0.7 and 3.5×10^{-9} cm^2/s in $Li_xCd[Fe(CN)_6]_{0.94}$ at x = 1.1. The D values for Na^+ were reported to be 0.5×10^{-10} cm^2/s in $Na_xCo[Fe(CN)_6]_{0.88}$ at x = 0.8, 2.3×10^{-10} cm^2/s in $Na_xMn[Fe(CN)_6]_{0.84}$ at x = 0.7, and 7.7×10^{-10} cm^2/s in $Na_xCd[Fe(CN)_6]_{0.94}$ at x = 1.1.

Among the PBAs, the Co-PBA film exhibits a remarkable color change from transparent green to dark violet upon deintercalation of alkali metal ions.[33,34)] In $Na_xCo[Fe(CN)_6]_{0.82}$ film[33)] at x = 1.28 (fully-reduced state), the absorption edge is below 490 nm reflecting divalent Co and Fe. In the range of $0.28 \leq x \leq 1.28$, Co^{2+} is oxidized to Co^{3+} with decrease in x from x = 1.28 (fully-reduced state). The oxidization of Co^{2+} causes an absorption band at 540 nm due to electron transfer from Fe^{2+} to Co^{3+}. The intensity of the 540 nm band increases with increase in the ratio (= 1.28 - x) of Co^{3+}. Then, the Na^+ concentration (x) can be evaluated by the spectral weight of the 540 nm band. $Li_xCo[Fe(CN)_6]_{0.90}$ shows a first order phase transition at x =1.2.[20)] Takachi *et al.*[35)] visualized the macroscopic phase separation during the charge process in thin film of $Li_xCo[Fe(CN)_6]_{0.90}$, using the characteristic 540 nm band. The corresponding Na compound ($Na_xCo[Fe(CN)_6]_{0.90}$; NCF90) shows no phase transition in the entire region of x.[23)] Then, it is possible to perform *in situ* monitoring of the Na^+ concentration (x) image in the NCF90 film by utilizing the 540 nm band. If we can prepare a stepwise initial distribution of x, we can clarify macroscale ($\gg \mu$m) Na^+ diffusion process agnist elased time (t). We call such an approached as transmission approach. In the EIS and SPM approaches, the D value is evaluated through the electric and/or volume response at specific position. This makes sharp contrast with the transmission approach, in which the D value can be evaluated by t-dependence of the entire distribution of x. In this sense, macroscopic D value can be evaluated by the transmission approach.

In this paper, we investigates the macroscopic Na^+ diffusion in thin film of NCF90 through the transmission approches. We found that the D value for Na^+ shows x-dependence as D = 6.0×10^{-8} - (1.6 - x)6.0×10^{-8} cm^2/s. The average D value (= 3.0×10^{-8} cm^2/s) is much larger than the reported value (= 0.5×10^{-10} cm^2/s[1)]) of $Na_xCo[Fe(CN)_6]_{0.88}$ (x = 0.8) film determined by the EIS analysis perpendicular to the film. The large D value evaluated in the present investigation is ascribed to the fast intergrain diffusion process.

Thin film of NCF90 was synthesized by electrochemical deposition on an indium tin oxide (ITO) transparent electrode under potentiostatic conditions at -0.45 V vs a standard Ag/AgCl electrode. The electrolytes were aqueous solution containing 0.8 mmol/L $K_3[Fe(CN)_6]$, 0.5 mmol/L $Co(NO_3)_2$, and 5.0 mol/L $NaNO_3$. In this process, the reduction reaction of $[Fe^{3+}(CN)_6]^{3-}$ triggers the deposition, and hence, Fe and Co in the as-grown films are divalent. The deposition time was 5 minutes. The obtained film was transparent green with a thickness of 0.23 μm. The chemical compositions of the films were determined using the inductively coupled plasma (ICP) method and CHN organic elemental analysis. The lattice constant (a) of the as-grown NCF90 film was a = 7.40(1) Å and c = 17.50(4) Å with trigonal distortion, which was evaluated by the X-ray diffraction pattern of the film. The lattice constants are consistent with literature.[32] The scanning electron microscopy (SEM) images were obtained using a SEM (JST-IT200; JEOL, Ltd.) at an acceleration voltage of 15 kV. The elemental map was obtained using an energy-dispersive X-ray spectrometer (EDS) installed in the SEM. The SEM image [Fig. 1(a)] reveals that the film consists of micro crystals of 0.4 μm in diameter.

To make a stepwise distribution of x, we performed initial oxidization process of the NCF90 film. Shibata *et al.*[36] reported that the contact area of two PBA thin films in the air is permeable to Na^+ but not to electrons. Therefore, we contacted the left half of the NCF90 thin film with a pre-oxidized NCF90 film (x = 0.0) film with a thickness of 0.92 μm. The pre-oxidization was performed using the same three-pole beaker-type cell,[34] whose working, counter, and referential electrodes were the NCF90 film, Pt, and a Ag/AgCl standard electrodes, respectively. The electrolyte was an aqueous solution of 17mol/kg $NaClO_4$. The charge rate was 1.5 C. Then, a current was applied to the contact area ar a rate of 1.5 C so that the NCF90 film was oxidized to x = 0.6. The pre-oxidized NCF90 film was then carefully removed. The color of the contact area changed into violet, reflecting the oxidization the NCF90 film. Figure 1(b) shows the elemental map of Na after the initial oxidization. A stepwise variation of the Na concentration is observed between the left and right half of the film. Since the left half of the film was oxidized (x = 0.6), the Na concentration is smaller in the left half. We confirmed that distributions of Fe [Fig. 1(c)] and Co [(d)] are uniform in the film.

Figures 2(a) shows transmitted light intensity image of the NCF90 soon after the initial oxidization. The film was placed in an atmospheric and dark place. The incident light was monochromated at 540 nm with a bandpass filter. The photon energy of the incident light was matched to the 540 nm band due to the electron transfer from Fe^{2+} to Co^{3+}. Weak intensity means a high degree of oxidation (small x). Since the left half of the film was oxidized (x =0.6), the transmitted light intensity is weak in the left half. Figures 2(b)-(d) shows the transmitted light intensity images against the elapsed time (t) after the initial oxidization. At (a) t = 1 h, the boundary between the left and right halves is slightly blurred. As t increases, the boundary becomes more blurred [(c) and (d)].

We evaluated the Na^+ concentration, $x(l, t)$, against the position (l) perpendicular to the initial boundary and elapsed time (t) from the corresponding absorbance A (= $-\ln\frac{I}{I_0}$, where I and I_0 are the transmitted light intensity and that without the film.). In the x range investigated ($0.6 \le x \le 1.6$), Co^{2+} is oxidized to Co^{3+} with decrease in x from x = 1.6 (fully-reduced state).[23] Recall that the 540 nm absorption band is due to the electron transfer from Fe^{2+} to Co^{3+}. Then, A increases in proportion to the ratio (= 1.6 - x) of Co^{3+}. To improve the S/N ratio, we performed a 649 point average of $x(l, t)$ parallel to the boundary. Here, we define the normalized absorption intensity A_n as $A_n = \frac{A-A_{1.6}}{A_{0.6}-A_{1.6}}$, where $A_{0.6}$ and $A_{1.6}$ are the A values at x = 0.6 and 1.6, respectively. Thus defined A_n is the same as x. We adopted the maximum and minimum A values as $A_{0.6}$ and $A_{1.6}$. Thus, we experimentally determined $x(l, t)$ and plotted them by crosses (t = 0 h), circles (1 h), triangles (2 h), and squares (3 h) in Figs. 3 and Figs. 4. The origin of l is set to the initial boundary.

The $x(l, t)$ data were analyzed by one dimensional (1D) diffusion equation, $\frac{\partial x}{\partial t} = \frac{\partial}{\partial l}(D\frac{\partial x}{\partial l})$. We introduces x-dependence of D as $D(x) = D_0 + (1.6 - x)D_1$. The 1D diffusion equation was calculated by the finite-difference method with a space mesh of 13.4 μm and a time mesh of 0.1 s. The experimental data at t = 0 h were used as the initial values. The calculations were performed in the region of -646 μm $\le l \le$ 609 μm with

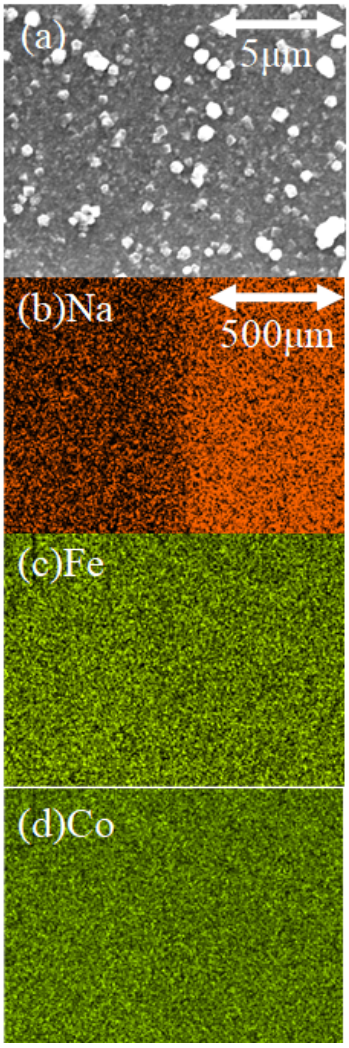

Fig. 1. (Color online) (a) Scanning electron microscopy (SEM) image of as-grown thin film of $Na_xCo[Fe(CN)_6]_{0.90}$ (NCF90). Elemental maps of the NCF90 film after the initial oxidization; (a) Na, (b) Fe, and (c) Co. The left side of the film was oxidized to x = 0.6.

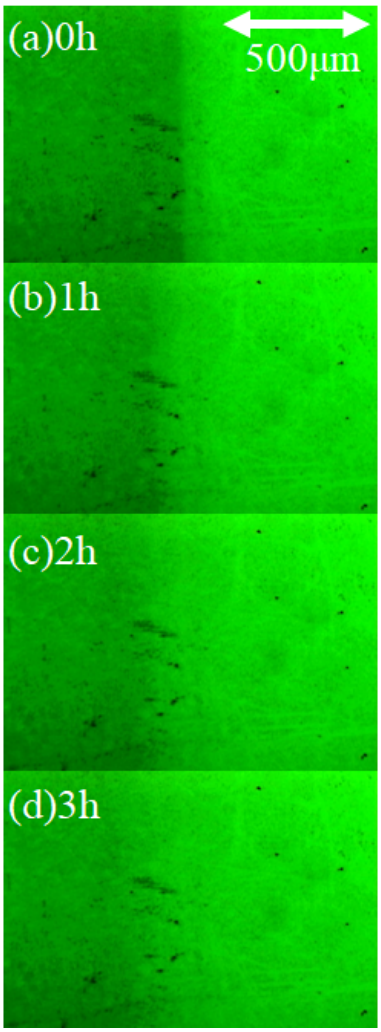

Fig. 2. (Color online) Transmitted light intensity image of the NCF90 film against the elapsed time (t) after the initial oxidization; (a) t = 0 h, (b) 1 h, (c) 2 h, and (d) 3 h. The left side of the film was oxidized to x = 0.6 at t = 0 h. The incident light was monochromated at 540 nm with a bandpass filter. The film was placed in an atmospheric and dark place. Contrast was linearly adjusted for visual aid.

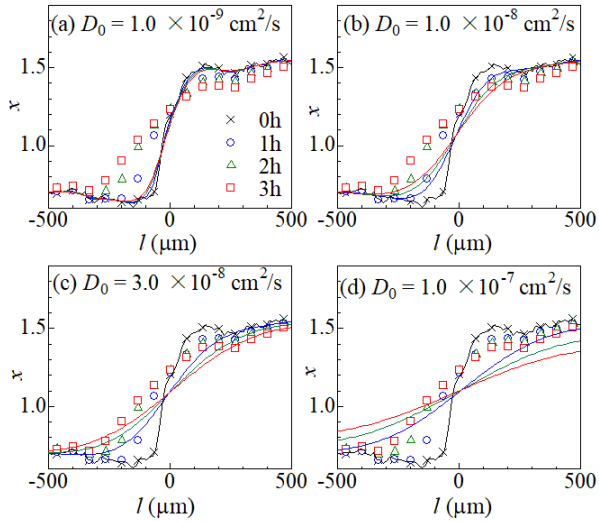

Fig. 3. Na^+ concentration (x) against position (l) perpendicular to the initial boundary and the elapsed time (t). Crosses, circles, triangles, and squares represent at t = 0, 1, 2, and 3 h, respectively. Solid curves are calculation results at different D_0 with fixing D_1 at zero: (a) D_0 = 1.0×10^{-9} cm^2/s, (b) 1.0×10^{-8} cm^2/s, (c) 3.0×10^{-8} cm^2/s, and (d) 1.0×10^{-7} cm^2/s.

the boundary condition that the number of Na^+ in the region is constant. We performed the calculations at several sets of D_0 and D_1.

Solid curves in Figs. 3 are the calculation results at different D_0 with fixing D_1 at zero: (a) D_0 = 1.0×10^{-9} cm^2/s, (b) 1.0×10^{-8} cm^2/s, (c) 3.0×10^{-8} cm^2/s, and (d) 1.0×10^{-7} cm^2/s. At (a) D_0 = 1.0×10^{-9} cm^2/s, Na^+ hardly diffuses even at t = 3 h. As D_0 increases, Na^+ diffusion becomes faster. At (d) D_0 = 1.0×10^{-7} cm^2/s, Na^+ diffuses to areas very far from the boundary even at t = 1 h. Crosses, circles, triangles, and squares are the experimentally obtained $x(l, x)$ at t = 0, 1, 2, and 3 h, respectively. The calculated curves at (a) D_0 = 1.0×10^{-9} cm^2/s and (d) D_0 = 1.0×10^{-7} cm^2/s fail to reproduce the experimental data. We investigated D_0-dependence of diffusion curve with fixing D_1 at zero. It was found that spatial extent of the Na^+ diffusion best matches the experimental data at (c) D_0 = 3.0×10^{-9} cm^2/s. In the region of -200 μm ≤ l ≤ 200 μm, however, the experimental data are larger than the calculated curves. In the following, we will adjust the D_1 value to better reproduce the experimental data in that region.

Solid curves in Figs. 4 are the calculation results at different D_0 and D_1. To keep the diffusion area nearly constant, the average $< D >$ value of D [= D_0 + (1.6 -x)D_1] was fixed at 3.0×10^{-8} cm^2/s: (a) D_0 = 3.0×10^{-8} cm^2/s and D_1 = 0.0×10^{-8} cm^2/s, (b) 4.0×10^{-8} cm^2/s and -2.0×10^{-8} cm^2/s,(c) 5.0×10^{-8} cm^2/s and -4.0×10^{-8} cm^2/s, (d) 6.0×10^{-8} cm^2/s and -6.0×10^{-8} cm^2/s. As D_1 decreases, the calculated curve swells upwards in the region of -200 μm ≤ l ≤ 200 μm and gradually approaches to the experimental data. We further investigated D_1-dependence of diffusion curve with fixing $< D >$ at 2.0×10^{-8} cm^2/s, 4.0×10^{-8} cm^2/s, and 5.0×10^{-8} cm^2/s. It was found that the diffusion profile best matches the experimental data at (d) D_0 = 6.0×10^{-8} cm^2/s and D_1 =-6.0×10^{-8} cm^2/s.

Thus determined $< D >$ value (= 3.0×10^{-8} cm^2/s) is much larger than the D value (= 0.5×10^{-10} cm^2/s.[1)]) in the $Na_xCo[Fe(CN)_6]_{88}$ film at x = 0.8. We note that the latter value was evaluated by the EIS analysis. in which the D value was evaluated from the frequency dependence of the complex impedance spectrum of the electrode and electrolyte system perpendicular to the film. The Na^+ diffusion process governs the profile of the impedance spectrum in the low frequency region (f ≤ 1 - 2 Hz). In the f region where the diffusion length (= $\sqrt{2Dt}$) is shorter than the grain size, the Nyquist plot shows a straight line with a slope of 1, reflecting the semi-infinite diffusion kinetics of Na^+. In the f region where the diffusion length becomes longer than the grain size, the plot becomes a vertical line, reflecting the finite diffusion kinetics of Na^+. Crudely speaking, D is on the order of $\frac{a^2}{f_c}$, where a and f_c are the grain radius and characteristic frequency where vertical line starts. Thus, the D value evaluated by the EIS analysis is dominated by the intragrain diffusion process. In the EIS approaches, the D value is evaluated through the electric response at specific position. This makes sharp contrast with the transmission approach, in which the D value is evaluated by t-dependence of the entire distribution of x. In the present investigation, the $< D >$ value was evaluated by the macroscopic spatial region (~ 500 μm) along the film direc-

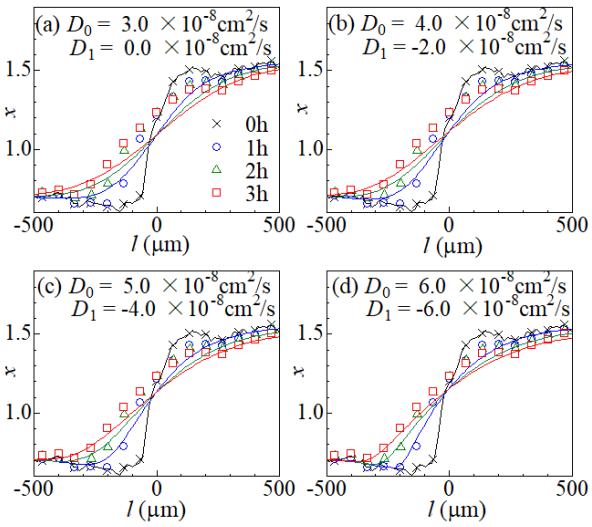

Fig. 4. Na^+ concentration (x) against position (l) perpendicular to the initial boundary and the elapsed time (t). Crosses, circles, triangles, and squares represent at t = 0, 1, 2, and 3 h, respectively. Solid curves are calculation results at different D_0 and D_1 with fixing the average value ($< D >$) of D [= D_0 + (1.6 -x)D_1] at 3.0×10^{-8} cm^2/s: (a) D_0 = 3.0×10^{-8} cm^2/s and D_1 = 0.0×10^{-8} cm^2/s, (b) 4.0×10^{-8} cm^2/s and -2.0×10^{-8} cm^2/s, (c) 5.0×10^{-8} cm^2/s and -4.0×10^{-8} cm^2/s, (d) 6.0×10^{-8} cm^2/s and -6.0×10^{-8} cm^2/s.

tion. The diffusion length (~ 100 μm) is much larger than the grain size (= 0.4 μm), and hence, the diffusion process consists of both the intergrain and intergrain components. Thus, the large $< D >$ value evaluated by the transmission approach is ascribed to the fast intergrain diffusion process.

Takachi *et al.*[24] reported that the discharge rate is 300 C for the NCF90 film with thickness of 1.1 μm. The 1D diffusion length (= 2.7 μm) calculated with the present $< D >$ (= 3.0×10^{-8} cm^2/s) and discharge time (= 1.2 s) is comparable to the film thickness (= 1.1 μm). The length (= 0.3 μm) calculated with D (= 0.5×10^{-10} cm^2/s), however, is smaller than the thickness. This argument suggests that the fast intergrain process play an important role in the discharge process of film electrode.

On the other hand, present analysis indicates that the D value decreases with decrease in x from x = 1.6 (fully reduced state). This x-dependence of D can be ascribed to the structural change induced by the oxidization of Co^{2+} to Co^{3+}. Reflecting the smaller ionic radius (= 0.55 Å) of the low-spin Co^{3+} as compared with that (= 0.75 Å) of the high-spin Co^{2+}, the lattice constant of NCF90 decreases from 10.15 Å at x = 1.6 to 9.95 Å at 0.6.[23] Such a shrinkage of the framework suppresses the Na^+ diffusion.

In conclusion, we investigated the Na^+ diffusion in the NCF90 film by means of transmitted light intensity images at 540 nm. We found that the D value for Na^+ shows x-dependence as D = 6.0×10^{-8} - (1.6 - x)6.0×10^{-8} cm^2/s. The average D value (= 3.0×10^{-8} cm^2/s) is much larger than the value (= 0.5×10^{-10} cm^2/s[1]) of $Na_xCo[Fe(CN)_6]_{0.88}$ (x = 0.8) film determined by the EIS analysis perpendicular to the film. The large D value evaluated in the present investigation is ascribed to the fast intergrain diffusion.

Acknowledgments

This work was supported by JSPS KAKENHI (Grant Numbers JP20J21687 and JP21H01822) and Murata Science Foundation.

1) M. Takachi, Y. Fukuzumi, and Y. Moritomo, Dalton Trans. **45**, 458 (2016).
2) A. Lasia. *Electrochemical impedance spectroscopy and its applications*, (Kluwer Academic/Plenum Pub., New Yprk, 1999), p. 143.
3) H. Xia, L. Lu, and G. Ceder, J. Power Sources **159**, 1422 (2006).
4) J. Xie, N. Imanishi, T. Zhang, A. Hirano, Y. Takeda, and O. Yamamoto, Electrochim. Acta **54**, 4631 (2000).
5) S. B. Tang, M. O. Lai, and L. Lu, Mater. Chem. Phys. **111**, 149 (2008).
6) T. Shibata, W. Kobayashi, and Y. Moritomo, Appl. Phys. Express **6**, 097101 (2013); *ibid.*, **8**, 029201 (2015).
7) S. Yang, B. Yan, L. Lu, and K. Zeng, RSC Adv. **6**, 94000 (2016).
8) K. Zeng, T. Li, and T. Tian, J. Phys. D **59**, 313001 (2017).
9) S. Yang, B. Yan, T. Li, J. Zhu, L. Lu, and K. Zeng, Phys. Chem. Chem. Phys. **17**, 22235 (2015).
10) J. Zhu, L. Lu, and K. Zeng, ACS Nano bf 7, 1666 (2013).
11) Y. Takahashi, T. Yamashita, D. Takamatsu, A. Kumatani, and T. Fukuma, Chem. Commmun. bf 56, 9324 (2020).
12) F. Xu, B. Beak, C. Jung, J. Solid State Electrochem. bf 16, 305 (2012).
13) J. Zhu, J. Feng, L. Lu, and K. Zeng,J. Power Sources **197** 224 (2012).
14) L. Danis, S. M. Gateman, C. Kuss, S. B. Schougaard, and J. Mauzeroll, Chem. Electro. Chem. **4**, 6 (2017).
15) M. Verdaguer, A. Bleuzen, V. Marvaud, J. Vaissermann, M. Seuleiman, C. Desplanches, A. Scuiller, C. Train, R. Garde, G. Gelly, C. Lomenech, I. Rosenman, P. Veillet, C. Cartier and F. Villain, Coord. Chem. Rev. **190-192**, 1023 (1999).
16) N. Imanishi, T. Morikawa, J. Kondo, Y. Takeda, O. Yamamoto, N. Kinugasa, and T. Yamagishi, J. Power Sources **79**, 215 (1999).
17) N. Imanishi, T. Morikawa, J. Kondo, R. Yamane, Y. Takeda, O. Yamamoto, H. Sakaebe, and M. Tabuchi, J. Power Sources **81-82**, 530 (1999).
18) M. Okubo, D. Asakura, Y. Mizuno, J.-D. Kim, T. Mizokawa, H. Kudo, I. Honnma, J. Phys. Chem. Lett. **1**, 2063 (2010).
19) T. Matsuda and Y. Moritomo, Appl. Phys. Express **4**, 047101 (2011).
20) M. Takachi, T. Matsuda, Y. Moritomo, Jpn. J. Appl. Phys. **52**, 044301 (2013).
21) Y. Lu, L. Wang, J. Cheng, and J. B. Goodenough, Chem. Commun. **48**, 6544 (2012).
22) T. Matsuda, M. Takachi, and Y. Moritomo, Chem. Commun. **49**, 2750 (2013).
23) M. Takachi, T. Matsuda, and Y. Moritomo, Appl. Phys. Express **6**, 025802 (2013).
24) M. Takachi, T. Matsuda, and Y. Moritomo, Jpn. J. Appl. Phys. **52**, 090202 (2013).
25) D. Yang, J. Xu, X.-Z. Liao, Y.-S. He, H. Liu, and Z.-F. Ma, Chem. Commum. **50**, 13377 (2014).
26) H. W. Lee, R. Y. Wang, M. Pasta, S. W. Lee, N. Liu, and Y. Chi, Nat. Commun. **5**, 5280 (2014).
27) L. Wang, J. Song, R. Q. Qiao, L. A. Wray, M. A. Hossain, Y.-D. Chung, W. Yang, Y. Lu, D. Evans, J.-J. Lee, S. Vail, X. Zhao, M. Nishijima, S. Kakimoto, and J. B. Goodenough, J. Am. Chem. Soc. **137**, 2548 (2015).
28) Y. You, X.-L. Wu, Y.-X. Yin, and Y.-G. Guo, J. Mater. Chem. A**1**, 14601 (2013).
29) S. Yu, Y. Li, Y. Lu, B. Xu, Q. Wang, M. Yan, Y. A. Jiang, J. Power Sources **275**, 45 (2015).
30) L. Xu, H. Li, X. Wu, M. Shao, S. Liu, B. Wang, G. Zhao, P. Sheng, X. Chen, Y. Han, Y. Cao, X. Ai, J. Qian, H. Yang, Electrochem. Commun. **98**, 78 (2019).
31) Y. Moritomo, S. Urase, T. Shibata, Electrochem. Acta **210**, 963 (2016).
32) Y. Moritomo, Y. Yoshida, D. Inoue, H. Iwaizumi, S. Kobayashi, S. Kawaguchi, and T. Shibata, J. Phys. Soc. Jpn., bf 90, 063801 (2021).
33) Y. Moritomo, H. Tachihara, H. Iwaizumi, T. Shibata, and H. Niwa, Jpn. J. Appl. Phys., bf 60, 040904 (2021).
34) I. Nagai, Y. Shimaura, T. Shibara, and Y. Moritomo, Appl. Phys. Express, **14**, 094004 (2021).

35) M. Takachi and Y. Moritomo, Sci. Reps., **7**, 42694 (2017).
36) T. Shibata, H. Kamioka, and Y. Moritomo, Jpn. J. Appl. Phys., **50**, 124101 (2011).